Effects of Rotor Deformation in Wind-Turbine Performance: The Dynamic Rotor Deformation Blade Element Momentum model (DRD-BEM)

Fernando L. Ponta[a,*], Alejandro D. Otero[b,a], Lucas I. Lago[a], Anurag Rajan[a]

[a] *Department of Mechanical Engineering - Engineering Mechanics, Michigan Technological University, Houghton, MI, 49931.*
[b] *CSC-CONICET & College of Engineering, University of Buenos Aires, Argentina.*

Abstract

Understanding the multi-physics phenomena associated with blade dynamics constitutes a fundamental factor for the continuous development of wind-turbine technology and the optimization of the efficiency of wind farms. Large size differences between wind-tunnel models and full scale prototypes preclude the proper extrapolation of experimental data, especially when several coupled physical phenomena are acting simultaneously; thus the need of an advanced Virtual Test Environment where innovative designs could be tested at reasonable computational cost.

We present a novel approach that we call the Dynamic Rotor Deformation - Blade Element Momentum model (DRD-BEM), which effectively takes into account the effects of the complex deformation modes of the rotor structure mentioned above. It is based on a combination of two advanced numerical schemes: First, a model of the structural response of composite blades, which allows full representation of the complex modes of blade deformation at a reduced computational cost; and second, a novel aerodynamic momentum model where all the velocities, forces, and geometrical features involved are transformed by orthogonal matrices representing the instantaneous deformed configuration, which fully incorporates the effects of rotor deformation into the computation of aerodynamic loads.

Results of validation cases for the NREL-5MW Wind Reference Turbine are presented and discussed.

Keywords:
Wind turbine, Innovative interference model, Blade aeroelastic modeling

1. Introduction

A better understanding of the multi-physics phenomena associated with blade dynamics constitutes a fundamental factor for the continuous development of wind-turbine technology

*Corresponding author
Email address: flponta@mtu.edu (Fernando L. Ponta)

and the optimization of the efficiency of wind farms. The complex combination of fluctuating loads under which blades operate, and the large size differences between wind-tunnel models and full scale prototypes preclude the proper extrapolation of experimental data, specially when several coupled physical phenomena are acting simultaneously. These are the reasons why advanced computer modelling of the interaction of the fluid, the structure, the control-system, and the electromechanical devices are so important to the design of innovative wind turbines, and to the optimization of their siting and operational procedures.

For many years, the wind-turbine industry has been increasing their use of computer models for rotor structural design and aerodynamic optimization. Nevertheless, the complex multi-physics interactions inherent to the coupled aeroelastic problem of rotor dynamics still challenge the capacities of available simulation codes. If the current tendency of the wind turbine market goes on, the size of the state of the art turbine will keep growing, and so the need of an advanced Virtual Test Environment where innovative turbine designs could be tested at full-scale conditions at reasonable computational cost.

This upscaling process may be accompanied by the introduction of lighter (and less stiff) blade designs that aim at reducing the costs of manufacture and materials, or the appearance of adaptive-blade designs where the aeroelastic modes of deformation are used to achieve control actions without the need for expensive actuators. Coupling between bending and twisting can be used to reduce extreme loads and improve fatigue performance (for a detailed discussion on the Adaptive-Blade concept see [1]). Thus, the next-generation of advanced wind turbine blades will likely be characterized by large displacements of the blade sections, either due to light-blade flexibility, adaptive bend-twist coupling design, or pre-conforming processes where specific curvatures are given to the blade axis *(i.e. coning-wise/sweeping-wise)*. Those displacements will be accompanied by large rotations of the blade sections whose alignment will no longer be perpendicular to the rotor's radial direction. All these factors point to a future scenario where the actual geometry of the wind-turbine rotor will change dynamically during normal operational conditions. This means that the actual rotor configuration will differ from the hypothesis on which the modelling theories commonly used today are based, and this situation will become worse as blades get more and more flexible.

Current techniques to simulate the aeroelastic dynamics of wind turbine blades range from using reduced-order models to full 3D ones in order to solve both problems, structure and aerodynamics, in a coupled way.

In reduced-order schemes, the structure is usually modeled as a Bernoulli or Timoshenko beam, either by means of space or modal discretization. Space discretization schemes are based in typical partial differential equation approximation methods like finite differences or finite elements. In modal discretization a limited finite number of deformation modes are kept in the solution. In both cases the continuous nature of the problem is dimensionally reduced from a 3D domain into a 1D one and the solution is obtained in a finite dimensional space. The selection of the method has direct effect on the accuracy and level of description of the simulated structural response. Reduced-order models for the flow problem are usually based on interference methods based on integral formulations of the flow equations in the form of conservation laws or on simplified flow equations, as in vortex methods. In the most common case, the flow problem is usually solved by some implementation of the well-known

Blade Element Momentum (BEM) model. Combining both structural and flow reduced models, a fully non-linear coupled scheme is obtained (see [2] for a comprehensive discussion). This technique gives origin to traditional aeroelastic approaches like the FAST-Aerodyn suite [3, 4, 5] or further developments like, for example, Kallesøe and Hansen [6], Xudong et al. [7]. Other implementations of reduced order models include different combinations of structural and flow models like Jeong et al. [8] or Yu and Kwon [9] where a full 3D flow model is combined with a beam structural model. Even though it is possible to do full 3D simulations for the flow problem in one hand, and 2D-shell or full-3D simulations for the blade structure on the other, where a higher level of description could be achieved for each physical aspect individually, a separate solution of the two physical phenomena misses crucial aspects of the coupled multi-physics problem that are essential for a complete representation of the blade dynamics. In addition, full-3D simulations of the coupled multi-physics problem (see, for example, Bazilevs et al. [10, 11]) as a whole are expensive in terms of computational cost, which limits the possibilities of simulating a large number of cases where different designs are tested in a variety of scenarios under different operational conditions and/or different control-strategies. The latter being very important in the search for optimization of the operational performance of the individual turbine. If we add to this the development of improved collective strategies for the wind-farm as a whole, the role of reduced-order models for the blade dynamics becomes even more important. Acting as Actuator Line Models (ALM) [12] integrated into a global flow scheme that simulates the flow domain of the entire wind farm, they offer the possibility of a feasible solution for whole-farm simulations without incurring a computational cost that would be prohibitive.

Thus, reduced-order aeroelastic models have the distinct advantage of providing a full insight into the actual coupled multi-physics dynamic, with less computational cost and a much faster solution. Nevertheless, the accuracy of classical reduced-order aeroelastic techniques is limited by the fact that both, the flow and the structural models, can only partially reflect the effects of the mutual feedback introduced, from one side, by the rotor deformation on the aerodynamic loads on the blade sections, and from the other, by the effect of that load change on the structural deformation itself. That is, important features affecting the coupling of the multi-physics problem (like blade section displacement and alignment) are still not fully represented.

To overcome these limitations and achieve a higher level of description, we developed a code based on a combination of two advanced numerical schemes: First, a model of the structural response of heterogeneous composite blades (see Otero and Ponta [13]), which allows a full representation of the complex modes of blade deformation and substantially reduces the computational effort required to model the structural dynamics at each time step. Second, a novel aerodynamic momentum model where all the velocities, forces, and geometrical features involved are transformed by orthogonal matrices representing the instantaneous deformed configuration, which fully includes the effects of rotor deformation into the computation of aerodynamic loads. This approach, which we call the Dynamic Rotor Deformation - Blade Element Momentum model (DRD-BEM), effectively takes into account the effects of the complex deformation modes of the rotor structure captured by the sophisticated structural model mentioned above; and it is the subject of the present paper.

2. The DRD-BEM model

2.1. Theoretical background and historical context

Since the 1970s several aerodynamic interference models have been proposed and extensively used in modelling both horizontal- and vertical-axis wind turbines. Models can be generally classified in two distinctive families: First, the Stream-Tube modelling family, based upon equating the forces on the blades to the change of momentum on one or more stream-tubes enclosing the swept area of the rotor (whose action is represented by one or more *actuator disks* placed across each tube); and second, the Vortex modelling family, based upon vortex representations of the blades and their wakes (see Ponta and Jacovkis [14] for a detailed historical discussion in the context of vertical axis rotors).

Among the models of the stream-tube family, we find the well known BEM model mentioned above, which is widely used in many applications dealing with the design and analysis of horizontal-axis wind turbine rotors (see [15] and [16] for a comprehensive description of the classical implementation of the BEM technique). Although originally proposed almost a century ago [17, 18], the BEM model is still a typical aerodynamic component on state-of-the-art approaches for the aeroelastic analysis of wind turbine rotors, a fact shown by the substantial amount of works published on the subject recently. Over the years, there have been improvements and corrections to achieve better results, but the basic BEM theoretical principles remain practically unchanged. Some examples of works published during the last decade which proposed modifications to the method include: Crawford [19] who analyzed the applicability of BEM theory for coning rotors Lanzafame and Messina [20] who considered different mathematical representations of the lift and drag coefficients and their effect when applied to BEM model. Lanzafame and Messina [21] who presented a way of including the effect of centrifugal pumping into BEM model modifying the lift coefficient, Madsen et al. [22] who proposed modifications of the BEM model comparing analytical and numerical results from other aerodynamical models, Dai et al. [23] who presented a modified Leishman-Beddoes [24] dynamic stall model in combination with BEM model, and Vaz et al. [25] who presented a model based on BEM theory for the horizontal-axis wind turbine design, taking into account the influence of the wake.

The classical mathematical formulation of BEM is based on a series of expressions using trigonometric functions to project velocities and forces, and it is constructed in such a way that implies the assumption of blade sections being perpendicular to a radial line contained in the rotor's plane. This means that classic BEM cannot take into account misalignments of the blade sections, which leads to a misrepresentation of the effects of the large deformations associated with flexible blades on the computation of aerodynamic forces. Moreover, the basics of the momentum theory remain valid when large deformations are present (i.e. , the principle of equating the aerodynamic forces on a set of blade elements to the change of momentum through a set of annular actuators associated with a corresponding set of concentric stream-tubes). Nevertheless, when the blade deforms, the thickness of the individual stream-tubes associated with each blade element are no longer constant, as the axis of the blade element also changes its alignment with respect to the radial line. This means that the area of the corresponding annular actuator will also be misrepresented. Hence, a new mathematical formulation is required to, first, project the velocities onto the the coordinate system aligned with the blade section, second, re-project backwards the resulting forces from the blade element onto the coordinate system aligned with the annular actuator, and third recalculate the area of the annular actuator in a way that takes into account the deformation of the rotor.

Like its classic counterpart, the DRD-BEM model presented here also belongs to the so-called stream-tube family of interference models. Nevertheless, a complete mathematical reformulation was developed to make it able to fully represent rotor-deformation effects at a level of description compatible with advanced structural models. The DRD-BEM can be thought of as a novel interference model of the stream-tube family on which all the aerodynamic effects associated with the misalignment of the blade airfoil sections, and the variations in shape, size, and orientation of the annular actuator are taking into account. As it was mentioned above, this is achieved by transforming the incident-velocity and the aerodynamic-force vectors through different coordinate systems. These start from the system aligned with the incident wind, up to the system aligned with the instantaneous position and attitude of the blade section (i.e. with axes defined by the chord-normal, chord-wise, and span-wise directions). These change-of-coordinate transformations are performed by a set of successive orthogonal matrices acting as linear operators. This technique allows us to automatically include not only the misalignment caused by instantaneous blade deformation and/or pre-conforming manufacturing processes, but also the misalignments caused by the action of the different mechanical devices that control yaw, pitch, and azimuthal (main shaft) rotation. Even changes in wind direction, and eventual design features like tilt- or coning-angle variations, could be included in the same way, using a consistent mathematical formulation for the whole set of phenomena. Hansen [26] also employed orthogonal matrices to compute the effects of yaw, tilt, and azimuthal rotation on wind velocities. As mentioned above, we add several more matrices to the chain of transformations to compute a full 3-D representation of the relative velocity field as seen by the blade element, as well as the backward transformation of the resulting forces and the area of the annular actuator, in a way that takes into account the deformation of the rotor.

Figure 1 shows a schematics of the instantaneous position of a generic blade element and its span-wise length, δl, which are projected into the hub coordinate system, h, defined according to the standards from the International Electrotechnical Commission (IEC) [27] (see figure 2, and the discussion about expressions 9 to 12 in section 2.4). Thus, the actual area of the annular actuator swept by the blade element, defined by the radial thickness δr_h and the radius r_h, is constantly updated. It is important to note that, even though we are aligning the h coordinate system with the hub, the stream-tube itself is going to be initially aligned with the direction of the incident wind, and then is going to be deflected after passing through the annular actuator. The amount of that deflection will depend on the forces exerted by the actuator on the flow particles (see discussion about expression 1 in section 2.4).

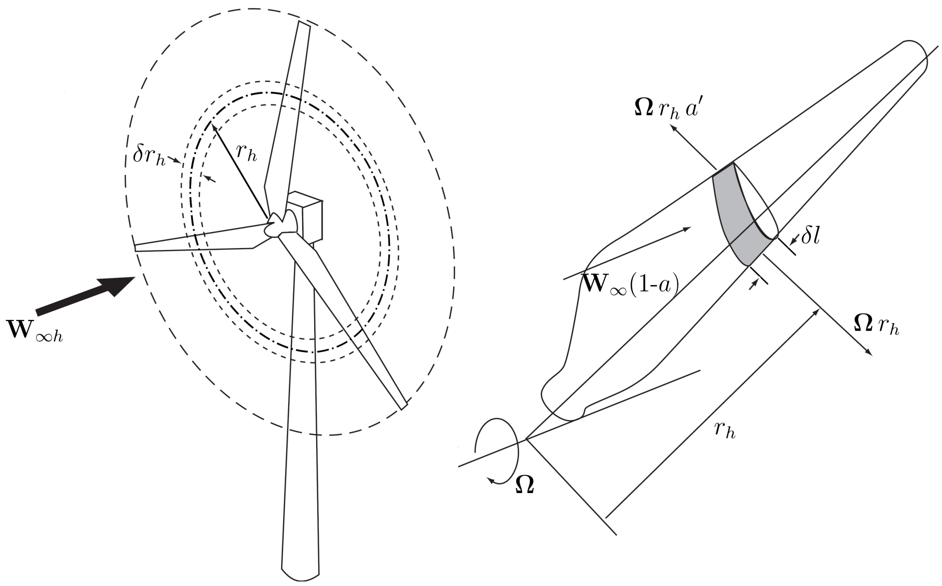

Figure 1: Schematic view of the dynamic generation of the annular actuator swept by a blade element (constructed in base on a scheme presented in Burton et al. [16] for the classical BEM formulation).

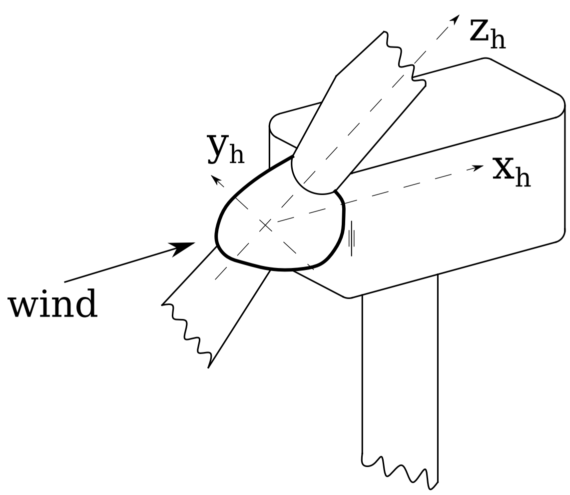

Figure 2: (b) Schematic representation of the hub coordinate system according to standards from the International Electrotechnical Commission (IEC) [27]

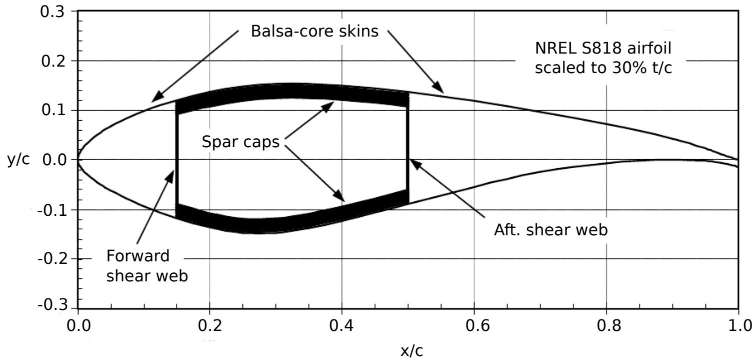

Figure 3: Example of a blade internal structure typical of current commercial types. The main structural member is a box-spar characterized by a significant build-up of material on the spar cap zone between the shear webs. The exterior shell and the shear webs are both of balsa-core sandwich construction with triaxial fiberglass laminate(from Griffin [28]).

2.2. Blade structural model: The dimensional-reduction technique for beams

Before describing in detail the procedure for the DRD-BEM, a brief account of the main features of the Generalized Timoshenko Beam Model (GTBM), which we used for the analysis of the blade structure, will be provided. For a detailed description of the implementation of our model and a comprehensive discussion on its historical background, the reader is referred to Otero and Ponta [13] and the references therein. That publication also includes results of the application of our code to the analysis of vibrational modes of composite laminate wind-turbine blades.

The need for advanced beam models stems from the fact that rotor blades are slender structures that may be studied as beams, which implies substantial savings in computational effort with respect to a full 3-D analysis. Nevertheless, due to the complex layout of their internal structure and the heterogeneous distribution of material properties (see figure 3 from Griffin [28], where a typical example of a blade internal structure is shown), blades are challenging to model by traditional beam theories (e.g. Bernoulli or standard Timoshenko). Moreover, because of their *ad hoc* kinematic assumptions, blade analysis by traditional beam theories may introduce significant errors, especially when they are vibrating at wavelengths that are shorter than their length [29]. The GTBM technique is designed to overcome these limitations.

Originally proposed by Prof. Hodges and his collaborators [30, 31], the GTBM is a dimensional reduction technique for complex beams that may have a curved and/or twisted shape that uses the same variables as the traditional Timoshenko beam theory, but where the hypothesis that the beam sections remain planar after deformation is abandoned. Instead, a 2-D finite-element mesh is used to interpolate the real warping of the deformed section, and a mathematical procedure is used to rewrite the strain energy of the 3-D body in terms of the classical 6 variables of the traditional 1-D Timoshenko theory for beams (i.e. the extensional strain, the two transverse shear strains, the torsional curvature, and the two bending curvatures). The complexity of the blade-section geometry and/or its material properties are reduced into a stiffness matrix for the equivalent 1-D beam problem, which is solved along a *reference-line*, L, that represents the axis of the beam on its original configuration (see figure 4). The procedure ensures that the strain energy of the reduced 1-D model is equivalent to the actual strain energy of the 3-D structure in an asymptotic sense.

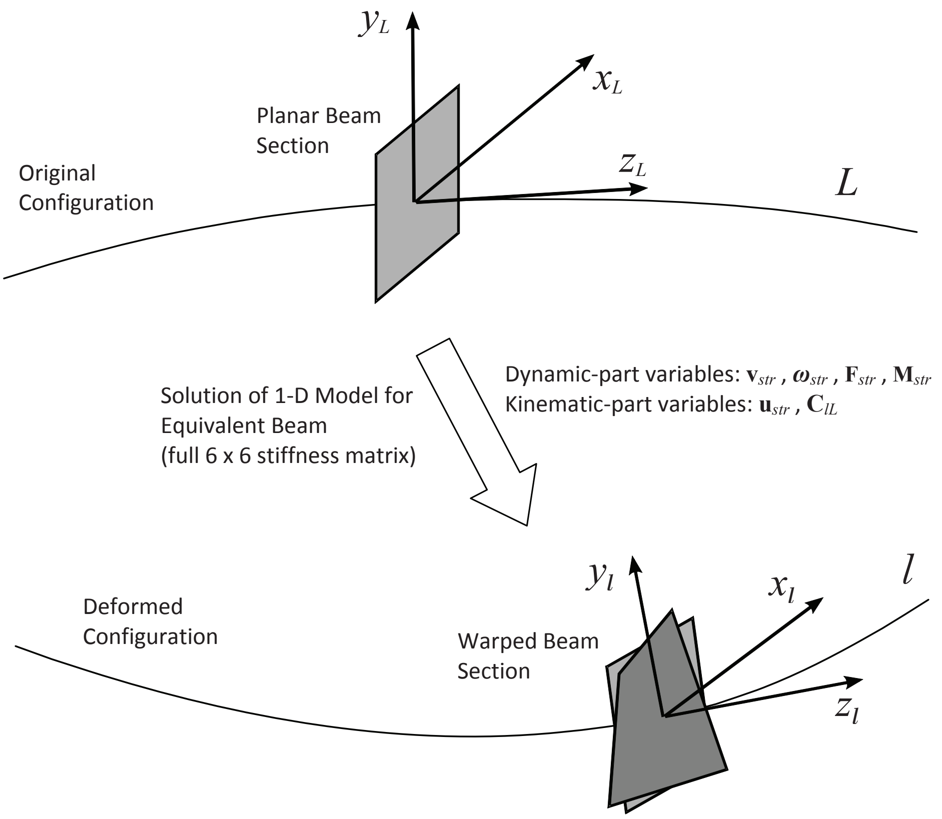

Figure 4: Schematic representation of the Generalized Timoshenko Beam Model for a generic beam section: views of the reference-lines, the beam sections, and the respective coordinate systems before and after deformation. The solution of the 1-D problem for the equivalent beam is indicated schematically, together with the variables involved in each one of its two parts. Note the warping of the originally planar section after deformation had occurred.

From the numerical point of view, elimination of the *ad hoc* kinematic assumptions of the traditional Timoshenko theory produces a fully populated 6x6 symmetric stiffness matrix for the 1-D beam, instead of only the 6 individual stiffness coefficients of the traditional theory. This means that now the 6 modes of deformation are fully coupled, and it is why this technique is referred to as a *generalized Timoshenko theory*. Thus, bending and transverse shear in two directions, extension, torsion, and the coupled modes of deformation (like bending-torsional or bending-bending) are fully represented in a consistent theoretical frame.

Essentially, through the GTBM we are able to decouple a 3-D nonlinear elasticity problem into a linear 2-D cross-sectional analysis (that may be solved *a priori*), plus a nonlinear 1-D unsteady problem for the equivalent beam that we solve at each time step of the aeroelastic analysis through an advanced ODE algorithm. The *a priori* 2-D analysis can be performed in parallel for many cross sections along the blade span, calculating the 3-D warping functions, and finding the stiffness matrix for the 1-D problem for the equivalent beam. Once the history of deformation for the ODE solution of the 1-D beam problem is obtained, the associated 3-D fields (displacements, stresses, and strains on the blade sections) at each time step can be recovered, *a posteriori*, using the 3-D warping functions calculated previously.

In figure 4, a system of coordinates intrinsic to the beam section, (x_L, y_L, z_L), is used to represent the kinematic and dynamic variables along the original reference-line L. The intrinsic system follows the deformation of the beam into the instantaneous configuration l to become (x_l, y_l, z_l). When this technique is applied to blades, the intrinsic system remains aligned to the blade sections in the chord-normal, chord-wise, and span-wise directions. Thus, even for the case of large displacements and rotations of the blade sections, this technique allows for accurate tracking of the position and alignment of the airfoil sections as a natural outcome of the solution of a 1-D finite-element problem. Besides, there are no constraints on the shape of the original reference line. L could be curved in any direction (i.e. twisted or bent), which allows modelling pre-conformed blades with a curved design (see further discussion about the $\mathbf{C}_{Lb}$ matrix on section 2.4).

The solution of the 1-D model for the equivalent beam, as schematically indicated in figure 4, is itself divided in two parts: one dynamic and one kinematic, each with their respective set of equations (see Otero and Ponta [13] for a comprehensive description, including the complete mathematical derivations).

The dynamic part is written in terms of 4 vectorial quantities (i.e. 12 variables): the so-called generalized velocities of vibration of the beam sections (which include the 3 linear velocities $\mathbf{v}_{str}$ and the 3 angular velocities $\boldsymbol{\omega}_{str}$); plus the so-called generalized forces on the beam section (which include the axial and the 2 shear forces $\mathbf{F}_{str}$, plus the torsional and the 2 bending moments $\mathbf{M}_{str}$). The 6 components of the generalized forces are directly related with the 6 variables of the Timoshenko theory through the 6x6 stiffness matrix for the equivalent beam mentioned above. The dynamic equations are essentially nonlinear, and could be either solved iteratively in a linearized mode to get steady-state solutions, or as a system of ordinary differential equations (ODEs) by means of an adaptive variable timestep ODE solver to get time dependent solutions.

The dynamic part of the solution also includes the inertia properties of the blade. Like the elastic properties discussed previously, these too are dimensionally-reduced to produce a 6×6 inertia matrix for the equivalent beam at each position along the reference-line. This matrix contains the mass per unit length, and the moments of inertia of first and second order for each blade section along the span. These are obtained from a two-dimensional integration performed over the area of each blade section which takes into account the details of its shape and its distribution of material properties. In this way, a full three-dimensional representation of the inertia properties of the blade are introduced into the dynamic solution. When operating in conjunction with the linear and angular velocities ($\mathbf{v}_{str}$, and $\boldsymbol{\omega}_{str}$), this matrix produces the 6 components of the linear and the angular momentum of the vibrational motion of the blade sections, and the inertia forces and moments associated with them. It also allows us to compute the inertia forces associated with the rotation of the main shaft and the action of mechanisms like yaw or pitch. Thus, centrifugal, Coriolis, angular, and linear acceleration effects are completely accounted for in a full three-dimensional representation (see also the discussion about the computation of gravitational forces in section 2.4).

The kinematic part uses as input the previous solution of the dynamic part to produce the displacements, $\mathbf{u}_{str}$, and the orthogonal matrices $\mathbf{C}_{lL}$ representing the rotations of the blade sections from the original configuration L to the deformed one l. The kinematic equations are highly nonlinear in nature due to the transcendental relations in the parametrization of rotations, and are solved through an iterative scheme, either at a steady-state condition, or at each step of a time-dependent solution from the ODE algorithm.

Matrix $\mathbf{C}_{lL}$, being updated at every timestep of the ODE solution of the structural model during dynamic simulations, is one of the key variables transferring information between the structural and the aerodynamic models, together with the displacements of the reference-line $\mathbf{u}_{str}$, and the linear and angular vibrational velocities of the blade sections ($\mathbf{v}_{str}$ and $\boldsymbol{\omega}_{str}$). On the other hand, aerodynamic load information coming from the aerodynamic model is fed into the structural 1-D solution by means of the distributed aerodynamic forces due to lift and drag and the aerodynamic pitch moment on the airfoil sections (this topic will be covered thoroughly on section 2.4).

2.3. The Common ODE Framework (CODEF)

Hitherto, we have seen how our structural model will interact with our aerodynamic model providing a comparable level of description to make full use of the advanced capabilities of both models. This notion of integral dynamic multi-physics modelling through an ODE solution in time could be extended to include other aspects that greatly affect the dynamics of the rotor and the overall performance of the wind-turbine, like the response of the control-system and/or the turbine's electromechanical devices.

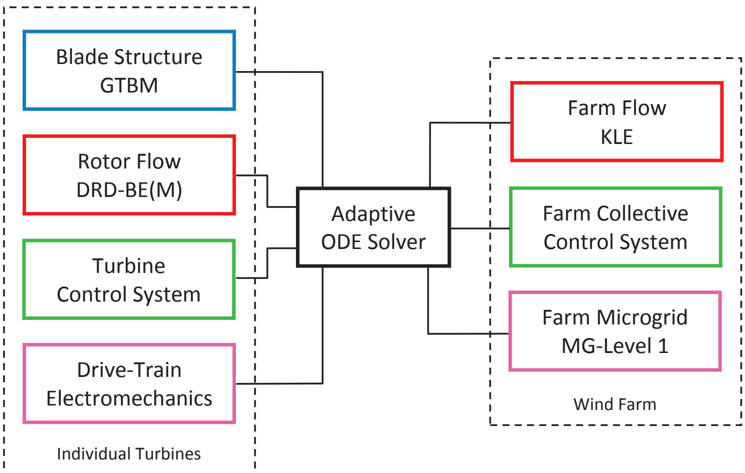

Figure 5: Flow-chart diagram of the Common ODE Framework.

As mentioned above, the equations of motion for the 1-D finite-element problem of the equivalent beam are solved using a nonlinear adaptive ODE solver. This type of solver is based on variable-timestep/variable-order ODE algorithms that check the solution by monitoring the local truncation error at every timestep, improving the efficiency and ensuring the stability of the time-marching scheme. The differential equations modeling the dynamics of the control system and electromechanical devices may be added to the general ODE system, with the control and the electromechanical dynamics modifying the boundary conditions for the aeroelastic solution and vice-versa. The use of a nonlinear adaptive ODE algorithm as a *common framework* provides a natural way of integrating the solution of all the multi-physics aspects of the problem. Figure 5 shows a flow-chart diagram of this global scheme indicating the interrelation between the different modules. These modules may be treated individually, interfacing with the common ODE routine. Contrary to a monolithic approach, this modular design of our multi-physics model substantially simplifies further development of the code by the improvement and/or expansion of each submodel independently. This makes possible the simultaneous analysis of the aeroelastic problem, together with any innovative control strategy involving all physical aspects of the turbine dynamics (mechanical and electrical), by means of an integral computationally-efficient solution through a self-adaptive algorithm. Moreover, it opens the door in the future for an interconnection of the dynamics of individual turbines into an integral simulation of their collective dynamics within a wind-farm, including all physical aspects of turbine-to-turbine interaction: aerodynamic, electrical, and collective control at farm-level.

2.4. DRD-BEM procedure

The procedure for the DRD-BEM algorithmic sequence consists of the following steps:

I **Modification of the incoming wind by the action of the annular actuator**

We shall start considering the velocity vector of the flow passing through an annular actuator aligned with the hub coordinate system h. The components of this velocity vector are affected by the axial induction factor a (i.e. , normal to the annular actuator) and the tangential induction factor a', representing respectively the axial velocity deficit and the increase in tangential velocity across the actuator. Then,

$$\mathbf{W}_h = \begin{bmatrix} W_{\infty h_x}(1-a) \\ W_{\infty h_y} + \Omega\, r_h a' \\ W_{\infty h_z} \end{bmatrix}, \tag{1}$$

is the velocity vector of the wind going through the annular actuator. $\mathbf{W}_{\infty h}$ is the undisturbed wind velocity field referred to the hub coordinate system, Ω is the angular velocity of the rotor, and r_h is the instantaneous radial distance as shown in figure 1. This three-dimensional construction of $\mathbf{W}_h$ reflects the fact that the concentric set of stream-tubes associated with each blade element is initially aligned with the incident wind direction expressed in the h system. Then, the action of the forces exerted by the annular actuators on the flow particles will alter their trajectory and deflect the stream-tubes accordingly, which is reflected in the change between the components of $\mathbf{W}_{\infty h}$ and $\mathbf{W}_h$ induced by the interference factors.

For the cases of rotors with tilt, and/or in the presence of changes in yaw angle and wind direction, the three-dimensional nature of $\mathbf{W}_{\infty h}$ will take those effects into account. To do this, we use a set of orthogonal matrices to transform the wind velocity defined in a coordinate system aligned with the wind itself, $\mathbf{W}_{\infty wind}$, into $\mathbf{W}_{\infty h}$.

Orthogonal three dimensional matrices work in a twofold manner: they can act as a linear operator transforming vectors between two coordinate systems, or as a mathematical representation of a rotation in the three-dimensional space (that is why they usually are simply referred to as *rotation matrices*). The case of coordinate transformation can be seen as a rotation of the first coordinate system to make it coincident with the second one.

The first orthogonal matrix that will transform $\mathbf{W}_{\infty wind}$ into $\mathbf{W}_{\infty h}$ is called $\mathbf{C}_{\Delta\theta_{yaw}}$, which will take into account any misalignment between the wind direction and the nacelle orientation, represented by the angle $\Delta\theta_{yaw}$, and is analogous to a rotation around the vertical axis. As a result, the wind velocity pre-multiplied by this matrix will be expressed into the *nacelle* coordinate system. This matrix has the form

$$\mathbf{C}_{\Delta\theta_{yaw}} = \begin{bmatrix} \cos(-\Delta\theta_{yaw}) & \sin(-\Delta\theta_{yaw}) & 0 \\ -\sin(-\Delta\theta_{yaw}) & \cos(-\Delta\theta_{yaw}) & 0 \\ 0 & 0 & 1 \end{bmatrix}, \tag{2}$$

where $\Delta\theta_{yaw} = \theta_{yaw} - \theta_\infty$, with θ_{yaw} the nacelle orientation and θ_∞ the direction of the unperturbed wind. The minus sign is due to the fact that $\Delta\theta_{yaw}$ is defined positive counter-clockwise according to IEC standards [27], and both θ_{yaw} and θ_∞ are defined positive in clockwise sense from the North as in a compass rose.

Next, we need to consider the vertical misalignment of the turbine axis introduced by tilt angle as defined by IEC standards [27] (see figure 6). The tilting matrix $\mathbf{C}_{\theta_{tlt}}$ involves a rotation around the horizontal axis of the *nacelle* system, transforming the velocity vectors into a coordinate system aligned with its first axis parallel to the turbine shaft. Then, the azimuthal orthogonal matrix $\mathbf{C}_{\theta_{az}}$ will transform the wind velocity into the *hub* coordinate system h of figure 2, by rotating the blade around the main shaft to its instantaneous position. This results on the expression for the unperturbed wind velocity referred to the hub coordinate system:

$$\mathbf{W}_{\infty h} = \left(\mathbf{C}_{\theta_{az}}\mathbf{C}_{\theta_{tlt}}\mathbf{C}_{\Delta\theta_{yaw}}\mathbf{W}_{\infty wind}\right). \tag{3}$$

II Projection of the velocity vector on the blade section coordinate system

Moving ahead from the hub's coordinate system, we add more matrices to the chain of transformations to compute the relative velocity as seen by the blade element. Thus, $\mathbf{W}_h$ will be projected going through several more coordinate systems, from the hub to the system aligned with the blade section.

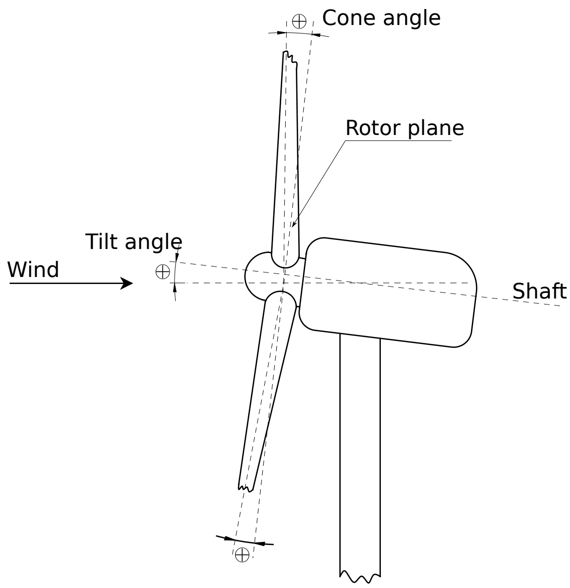

Figure 6: Definition of cone and tilt angles for upwind wind turbines, according to standards from the International Electrotechnical Commission (IEC) [27]

The coning transformation matrix $\mathbf{C}_{\theta_{cn}}$ is a linear operator taking into account the coning angle for the rotor (see figure 6), and is characterized by a rotation around the second axis of the hub coordinate system. This could be a fixed angle representing the coning of the rotor as a constructive feature (as in the case of the NREL-5MW reference wind turbine [32]) or, if a control mechanism based on changing the coning angle is included, a variable matrix reflecting any control action in real time; we have included both options in our code. For a detailed description of the concept of coning rotors and their effects see Jamieson [33], Crawford [19], Crawford and Platts [34].
Similarly, the pitching transformation matrix $\mathbf{C}_{\theta_p}$, is related to a rotation around the pitch axis of the blade, which is the third axis of the coordinate system resulting from the previous coning transformation. The pitch angle θ_p reflects any change in pitch introduced by the actuators of the control system. This leads to the so-called *blade* coordinate system indicated by the b subscript according to IEC standards [27] (see figure 7).

$$\mathbf{C}_{\theta_\mathbf{p}} = \begin{bmatrix} \cos(-\theta_p) & \sin(-\theta_p) & 0 \\ -\sin(-\theta_p) & \cos(-\theta_p) & 0 \\ 0 & 0 & 1 \end{bmatrix}, \tag{4}$$

with $\theta_p = \theta_{p_0} + \theta_{p_{ctrl}}$, the pitch angle, composed by θ_{p_0}, a fixed angle set up as a constructive feature, and $\theta_{p_{ctrl}}$, the pitch angle varied by the control system. The minus sign appears here due to the sense in which positive pitch angles are defined in the IEC standards.
This same scheme combining as needed a set-up and a control angle could be used within

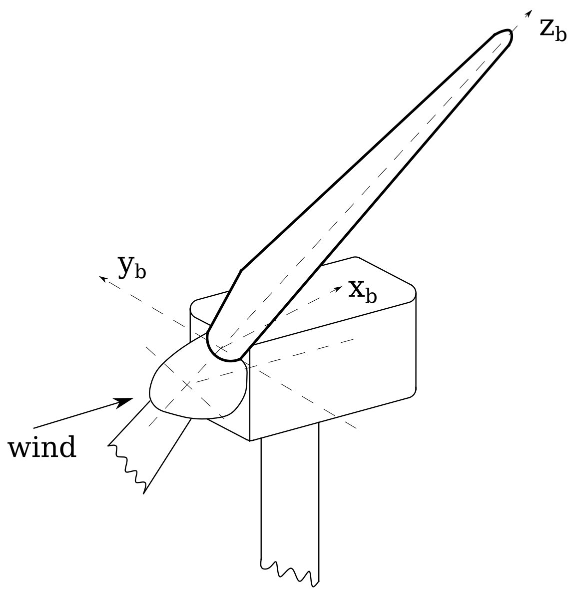

Figure 7: Blade coordinate system according to standards from the International Electrotechnical Commission (IEC) [27]

the tilt transformation $\mathbf{C}_{\theta_{tlt}}$, for turbines that use tilting as a control mechanism. The interaction with control and/or electromechanical modules requires a constant update of the projection matrices associated with mechanical devices. For example, the azimuth matrix $\mathbf{C}_{\theta_{az}}$, besides being used to compute the instantaneous position of the blade during its rotation, can also reflect control actions on the dynamics of the electromechanical drive train that affect the rotor's angular speed Ω.

In order to get to the coordinate system of the blade section in the instantaneous deformed configuration, (x_l, y_l, z_l), defined along the deformed reference-line l (see figure 4), two more transformations are applied after $\mathbf{C}_{\theta_\mathbf{p}}$:

The orthogonal matrix associated with the first of these transformations is based on the geometrical alignment of the blade sections along the span defined at the time when the blade was designed and manufactured. As previously mentioned, the blade could have pre-conformed curvatures along its longitudinal axis (i.e., the design blade axis is no longer rectilinear and the coordinate systems of different blade sections along the reference line are no longer aligned with the third axis of system b in figure 7). As mentioned above, the intrinsic system L is defined aligned to the blade sections in the chord-normal, chord-wise, and span-wise directions. Thus, the abovementioned curvatures can reflect either an initial twist along the longitudinal axis (which, in the case of a rectilinear blade, coincides with the classical notion of twist of standard BEM theory), or a combination of twist plus pre-bending on the other two axes (i.e. coning-wise/sweeping-wise). To this end, we compute a transformation orthogonal matrix for each position along the original reference line L, which we call $\mathbf{C}_{Lb}$, as it relates the coordinate system of the blade b with the intrinsic system of coordinates of the blade sections in the original (non-deformed) configuration (x_L, y_L, z_L) defined along line L. The orthogonal matrix associated with the second transformation mentioned above, $\mathbf{C}_{lL}$, is the one provided by the solution of the kinematic equations on the structural model (as explained in section 2.2), which transforms vectors from system L to system l. After all these transformations, the velocity vector $\mathbf{W}_h$ is expressed into the coordinate system of the blade section, and then we add the blade section vibrational velocities $\mathbf{v}_{str}$ coming from the structural model, which are already expressed in the l system. At this point, we also add the velocity components $\mathbf{v}_{mech}$, associated with the motion of the blade section due to the combined action of mechanical devices (like yaw, pitch, and azimuthal rotation), also expressed in the l system. Thus, the expression for the wind velocity relative to the blade section, $\mathbf{W}_l$, results:

$$\mathbf{W}_l = \left(\mathbf{C}_{lL}\mathbf{C}_{Lb}\mathbf{C}_{\theta_p}\mathbf{C}_{\theta_{cn}}\mathbf{W}_h\right) + \mathbf{v}_{str} + \mathbf{v}_{mech}. \tag{5}$$

III Computation of the aerodynamic forces from the *Blade Element Theory*

With the magnitude of the wind velocity projection onto the plain of the blade section, $W_{rel} = \sqrt{{W_{l_x}}^2 + {W_{l_y}}^2}$, and the angle of attack α, the aerodynamic lift and drag forces per unit length of span are computed in the classic way through the aerodynamic coefficients of the airfoil section:

$$dF_{lift} = \frac{1}{2}\rho\, C_l\, {W_{rel}}^2\, c\,, \qquad\qquad dF_{drag} = \frac{1}{2}\rho\, C_d\, {W_{rel}}^2\, c, \tag{6}$$

where C_l and C_d are the lift and drag coefficients for the corresponding angle of attack, ρ is the air density, and c is the chord length of the airfoil section. The total aerodynamic load acting on the blade element aligned with relative wind direction has components corresponding to the lift and drag forces and is given by

$$\delta\mathbf{F}_{rel} = \begin{bmatrix} dF_{lift} \\ dF_{drag} \\ 0 \end{bmatrix} \delta l, \tag{7}$$

where δl is the span length of the blade element as shown in figure 1.

IV Projection of the aerodynamic forces back to the hub coordinate system

The aerodynamic load $\delta\mathbf{F}_{rel}$ is then projected back onto the h coordinate system by reverting the transformation process using the inverse of the same orthogonal matrices explained before applied in reversed order. One interesting (and very useful) property of orthogonal matrices is that their inverse is equal to their transpose. Hence, the aerodynamic load on the blade element expressed in h coordinates is

$$\boldsymbol{\delta}\mathbf{F}_h = \mathbf{C}^T_{\theta_{cn}}\mathbf{C}^T_{\theta_p}\mathbf{C}^T_{Lb}\mathbf{C}^T_{lL}\mathbf{C}_{Lthal}\,\mathbf{dF}_{rel}\,\delta l, \tag{8}$$

where $\mathbf{C}_{Lthal}$ is the matrix that projects the lift and drag forces onto the chord-normal and chord-wise directions, which are aligned with the coordinates of l. Expression (8) could be re-written as $\boldsymbol{\delta}\mathbf{F}_h = \mathbf{dF}_h\,\delta l$, or in components

$$\boldsymbol{\delta}\mathbf{F}_h = \begin{bmatrix} \delta F_{h_x} \\ \delta F_{h_y} \\ \delta F_{h_z} \end{bmatrix} = \begin{bmatrix} dF_{h_x} \\ dF_{h_y} \\ dF_{h_z} \end{bmatrix} \delta l, \tag{9}$$

where $\mathbf{dF}_h = \mathbf{C}^T_{\theta_{cn}} \mathbf{C}^T_{\theta_p} \mathbf{C}^T_{Lb} \mathbf{C}^T_{lL} \mathbf{C}_{Lthal}\,\mathbf{dF}_{rel}$.

V Equating forces from *Blade Element Theory* and *Momentum Theory*

Finally, the components of the force coming from the blade element theory $\boldsymbol{\delta}\mathbf{F}_h$ are equated to the rate of change of momentum through the corresponding annular actuator. The component normal to the annular actuator δF_{h_x}, is equated to the change in momentum on $W_{\infty h_x}$ associated with the axial interference factor a (see expression 1), which after some algebraic manipulation gives

$$dF_{h_x} = f_{th}\frac{4\pi\,\rho\,r_h}{B}\left(W^2_{\infty h_x}\,a\,(1-a) + (a'\Omega\,r_h)^2\right)\frac{\delta r_h}{\delta l}, \tag{10}$$

where f_{th} is the combination of the tip and hub loss factors described later in section 2.5, and B is the number of blades of the rotor. Here we included the term $(a'\Omega\,r_h)^2$, which takes into account the fact that the rotation of the wake causes a pressure drop behind the actuator equal to the increase in dynamic head [16]. The term $\frac{\delta r_h}{\delta l}$ involves the transformation of δl into δr_h referred to in section 2.1, which is performed by means of the same set of orthogonal matrices already described.
The tangential component δF_{h_y}, is then equated to the corresponding change momentum associated with induction factor a' which gives

$$dF_{h_y} = f_{th}\,\frac{4\pi\,\rho\,r_h}{B}\,|W_{\infty h_x}|\,(1-a)\,(\Omega\,r_h)\,a'\,\frac{\delta r_h}{\delta l}. \tag{11}$$

VI Iterative solution for the induction factors

As in the classic BEM, the set of equations (10) and (11) form a nonlinear system where the unknowns are the two induction factors a and a', which needs to be solved by an iterative process within each timestep of the aeroelastic solution for each one of the blade elements. In traditional implementations of BEM, this is usually solved by functional iteration schemes starting from an initial guess value. Given the more complex nature of the DRD-BEM, we decided to use an advanced optimization algorithm to improve the stability and the speed of convergence of the iterative process. To this end, we rewrote equation (10) into an implicit expression for a,

$$a_{Res} = dF_{h_x} - f_{th}\frac{4\pi\,\rho\,r_h}{B}\left(W^2_{\infty h_x}\,a\,(1-a) + (a'\Omega\,r_h)^2\right)\frac{\delta r_h}{\delta l}, \tag{12}$$

and equation (11) into an explicit expression for a'

$$a' = \frac{dF_{h_y}\, B}{f_{th}\, 4\pi\, \rho\, r_h\, |W_{\infty h_x}|\, (1-a)\, (\Omega\, r_h)\, \frac{\delta r_h}{\delta l}} \tag{13}$$

Then, we solve for the axial induction factor a, finding the zero of equation (12) by minimizing its residual a_{Res}, with expression (13) providing an update of a' at each step of the iteration process that acts as a constraint. For the minimization of the residual we use an adaptive algorithm based on a combination of bisection, secant, and inverse quadratic interpolation methods. The main advantage of applying this close-interval method, instead of the traditional iteration from an initial guess value, is that the search is always bracketed between two limiting values that enclose the range where the solution is expected. Thus, it avoids the situation where the solution overshoots and diverges, or gets trapped into an endless loop. In this way, the convergence criteria, as well as the error check, is constantly monitored by an efficient, proven, and highly reliable numerical scheme [35, 36].

VII Computation of the distributed loads on the blade structure

The next step in the process is to compute the distributed loads and moments acting on the blade structure per unit length of span. These forces, expressed on the intrinsic system of coordinates at the instantaneous configuration l, constitute the input required by the GTBM structural model (see section 2.2). The distributed loads have two main components: one associated with the aerodynamic forces, and the other with the gravitational action.

Once the iterative solution for the induction factors in step VI achieves convergence, we are able to compute the aerodynamic forces acting on each blade section by following part of the process from steps I to III, but this time expressing them in system l, that is $\mathbf{dF}_l = \mathbf{C}_{Lthal}\, \mathbf{dF}_{rel}$, whose first two components give the chord-normal and the chord-wise aerodynamic loads. To these forces we add the aerodynamic moment on the airfoil section per unit span-length, which acts around the first axis of l, and is computed through the classic formula using the aerodynamic pitch coefficient C_m of the airfoil section at the corresponding angle of attack $dM_{aer} = \frac{1}{2}\rho\, C_m\, {W_{rel}}^2\, c^2$.

The three-dimensional contribution of the gravitational action to the distributed forces and moments along the span is computed for the instantaneous position and attitude of each blade section. To this end, we use the same inertia properties included in the 6×6 dimensionally-reduced inertia matrix for the equivalent beam, previously described in section 2.2. Our code has the capacity to switch the gravitational load on or off according to the preferences of the user.

With these inputs, the structural model is able to produce the dynamic and kinematic variables to characterize the rotor deformation, and we then proceed to the next iteration of the process.

2.5. Dynamic update of corrective factors

The implementation of the DRD-BEM also contains some additional improvements in the form of a dynamic update of correction factors, which in traditional versions of BEM, were pre-computed and kept constant along the calculation. Namely:

- Airfoil aerodynamic data from static wind-tunnel tests are corrected at every timestep to consider both rotational-augmentation and dynamic-stall effects. The rotational-augmentation correction is based on the well-know models of Du and Selig [37] and Eggers [38]. The dynamic-stall model we use is based in the works of Leishman and Beddoes [24], Leishman et al. [39] and Leishman and Beddoes [40]; and our code has the capacity of switching between three options for its application: It could be applied at each step of the iterative solution for the interference factors plus at the computation of the aerodynamic loads (i.e. at steps III and VII); it could be applied only during the computation of the aerodynamic loads after the iterative solution have converged (i.e. only at step VII); or it could be totally switched off.

- Our code is capable of using multiple data tables for the aerodynamic coefficients of the airfoil sections. These multiple data sets could be associated with different Reynolds numbers, with the actuation of flow-control devices (like flaps, ailerons, tabs, or spoilers), or with any other factor that modifies the original curves of coefficients versus angle of attack. The data on the tables are interpolated at every time-step providing coefficient values updated to account for the instantaneous aerodynamic conditions and/or control actions on the flow-control devices. This feature opens interesting possibilities for future studies that we discuss on the concluding section.

- To ensure the availability of data for a range of angles of attack $\pm 180°$, we use the well known extrapolation method proposed by Viterna and Janetzke [41], which is also applied in real-time like the other corrections previously mentioned (i.e. they are applied at every computation of the aerodynamic forces made in steps III and VII).

Our model also incorporates several empirical corrections that are typically present in state-of-the-art BEM models [see 15, 16]:

- BEM theory does not account for the influence of vortices being shed from the blade tips into the wake on the induced velocity field. These tip vortices create multiple helical structures in the wake which play a major role in the induced velocity distribution at the rotor. To compensate for this deficiency in BEM theory, a tip-loss model originally developed by Prandtl is implemented as a correction factor to the induced velocity field [18]. In the same way, a hub-loss model serves to correct the induced velocity resulting from vortex being shed from the blade roots at the rotor hub. Both are condensed in the f_{th} factor included in equations (10) to (13).

- Another modification needed in any model based on momentum theory is the correction of the thrust on the annular actuator when operating in the so-called "turbulent-wake"

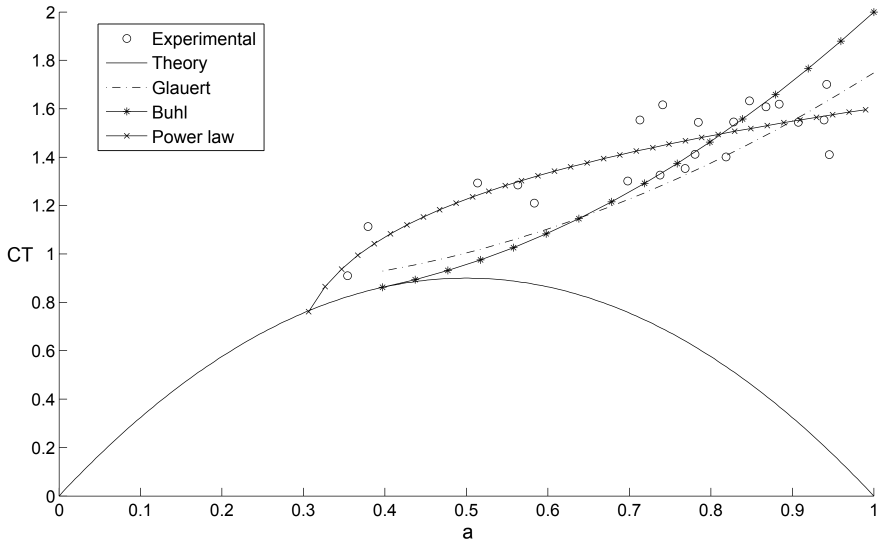

Figure 8: Graphical representation of the thrust coefficient CT in function of the axial induction factor a. The parabolic curve given by conservation of momentum in the stream-tube; Glauert [17] and Buhl [42] empirical relations fitting Lock et al. [43] experimental data; and the Power-Law fitting proposed here to minimize the error. The parabolic CT curve form stream-tube theory is shown here affected by a tip-hub loss factor $f_{th} = 0.9$ to illustrate the gap-problem on the Glauert approach.

state. This correction plays a key role when the turbine operates at high tip speed ratios and the axial induction factor a is greater than 0.5 (in practical implementations, this limit is lowered to about 0.3 to 0.45, depending on the corrective curve adopted). At $a = 0.5$, the parabola representing the thrust coefficient CT as a function of a reaches its vertex (see figure 8), and beyond that, the basic assumptions of momentum theory on a stream-tube become invalid as part of the flow in the far wake starts to propagate upstream. Physically, this flow reversal cannot occur and what actually happens is that more flow entrains from outside of the wake, creating vortex structures and increasing the turbulent activity. This slows down the flow passing through the rotor, but the thrust continues to increase.

Glauert [17] was the first to propose an empirical correction to overcome this limitation in momentum theory. He fitted a parabolic function to the experimental data from Lock et al. [43] for wind turbines operating in the turbulent wake state. Glauert's fitting function is tangent to the stream-tube CT curve at $a = 0.4$ (see figure 8). Other authors such as Burton et al. [16] and Wilson [44] also proposed alternative fitting functions to the experimental data. Nevertheless, a discontinuity between the fitting function and the stream-tube CT function appears when correction factors for tip and hub losses are taken into account [42]. This discontinuity becomes critical when the induction factors are to be obtained by iterative approaches. Buhl [42] proposed a new empirical relationship for the thrust coefficient that solves the gap-problem by ensuring a tangent matching with the stream-tube CT function regardless if it is affected by corrective factors for tip and hub losses.

Our model is able to employ different empirical relations fitting the experimental data by Lock et al. [43], that could be chosen by a switch in the input. We also introduced a new corrective curve based on a Power-Law fitting, which substantially reduces the error of approximation to Lock et al. [43] empirical data and also avoids the gap-problem as the Power-Law fitting always intercepts the stream-tube CT function regardless of the corrective factors for tip and hub losses applied. A full discussion on this newly-proposed Power-Law fitting will be the object of a separate paper, as it fairly exceeds the scope of the present work. Both Buhl [42] curve and our Power-Law fitting are shown in figure 8.

- The influence of the tower on the flow field around the blade must also be modelled. We use the models developed by Bak et al. [45] and Powles [46], which provide the influence of the tower on the local velocity field at all points around it. These models account for the increase in wind speed around the sides of the tower, the appearance of cross-stream velocity components, the deceleration of the flow at the stagnation zone upstream of the tower, and the velocity deficit in the separated wake behind it in case the rotor operates in a downwind configuration.

3. Numerical Experimentation

In this section, we report results of the application of our model to the aerodynamic analysis of a rotor based on the *5-MW Reference Wind Turbine (RWT)* proposed by NREL [32]. Based on the REpower 5M wind turbine, the NREL's RWT was conceived as a benchmark turbine for both onshore and offshore installations, and it is a good representative of state-of-the-art, utility-scale, multi-megawatt commercial wind turbines. An earlier version of the DRD-BEM called the LSR-BEM model was used in combination with the GTBM structural model (section 2.2) for the analysis of the aeroelastic steady state and the deformation modes of the NREL-RWT's blades in Otero et al. [47]; and to analyze the performance of alternative adaptive designs for the the NREL-RWT blade in Lago et al. [48].

3.1. Power and Thrust

According to Jonkman et al. [32], the NREL-RWT's blades are designed to be actuated for pitch control only for wind speeds beyond the nominal (rated) value $W_N = 11.4$ m/s, where the goal is to maintain a constant power output and a constant angular speed of the rotor. During operation at wind speeds lower than the rated, the pitch remains constant at its design value, and the angular speed of the rotor is controlled to keep the tip speed ratio at the nominal value of $\lambda = 7$.

The first series of results shows the outcome of our model analyzing the blade under steady-state operational conditions when the effects of aeroelastic deformation are included. We ran tests for operational conditions at different wind speeds ranging from 3 m/s to 25 m/s which are, respectively, the cut-in and cut-out design wind speeds for the NREL-RWT. Figure 9 shows the power output at different wind speeds, the thrust at the hub, and the power and thrust coefficients. As a validation of our model, we compare results of the present study with results for steady state power and thrust from Jonkman et al. [32] and Xudong et al. [7]. Jonkman et al. [32] results were obtained by means of the certified FAST-Aerodyn suite [3, 4, 5], which are based on the BEM formulation combined with a modal beam method for the structural analysis. The work of Xudong et al. [7] presents a method for optimizing wind turbine rotors, that relies on their own aeroelastic model to simulate the turbine behavior. This aeroelastic model is also based on a combination of BEM and modal structural model and was validated against the FLEX code [49].

Below W_N, we applied a rotational speed that gave the design tip speed ratio at the corresponding wind speed. Above W_N, we computed the pitch control angle for the blades at every wind condition that keep both the power output and rotor speed constant at their nominal values. In order to strictly reproduce an actual steady-state condition, tilt and yaw angles need to be disregarded, as well as the action of gravitational forces. All these factors introduce asymmetries in the blade structural loads inducing unsteady aeroelastic behaviour along the turning cycle, which our model is capable of detecting. Thus, we applied the NREL-RWT's design tilt angle of 5° [32] only for our time-dependent solutions (shown later), while the results for steady-state solutions where obtained in the absence of tilt. A hub-coning angle of 2.5° was applied as specified in the definition of the NREL-RWT's constructive parameters [32].

At nominal operational conditions, the mechanical power at the rotor's shaft predicted by our model is 5.1916MW. This is slightly lower than the value reported in Jonkman et al. [32], which is consistent with the fact that the structural deformation, and the misalignment it induces on the blade's airfoil sections, is now taken into account (see also comments on section 4).

Rotor power results reported by Xudong et al. [7] are similar to our results for most wind speeds, while thrust results of both models are slightly higher than ours. This, again, is consistent with the fact that none of those models take into account the misalignment of the airfoil sections. In table 1, we present results obtained with our model for the tip deflection both in and out of the rotor plane. Our results are compared with those of Jonkman et al. [32], Xudong et al. [7], Jeong et al. [8], Kallesøe and Hansen [6], and Yu and Kwon [9]. The method used by Jeong et al. [8] combines a free wake vortex model with a finite-element beam formulation. Kallesøe and Hansen [6] use a nonlinear steady state version of the second order Euler-Bernoulli beam model coupled with a BEM model to compute steady state blade deformations. Yu and Kwon [9] use an incompressible Navier–Stokes computational fluid dynamics solver based on unstructured meshes to solve the flow field around the turbine. This method was combined with a nonlinear Euler-Bernoulli cantilever beam undergoing spanwise, lead-lag bending, flap bending, and torsional deformations discretized by the finite-element method to model the blade structure. The majority of the methods agree quite well in terms of the out-of-plane displacement, while the in-plane deflection values are more dispersed. As can be seen there is a wide variety of options among the fluid solvers found in the literature, but structural models are restricted to classical beam formulations. This could be the reason for the different behavior observed for the in-plane and the out-of-plane deflections, classical formulations seem to work well for the out-of-plane direction where the

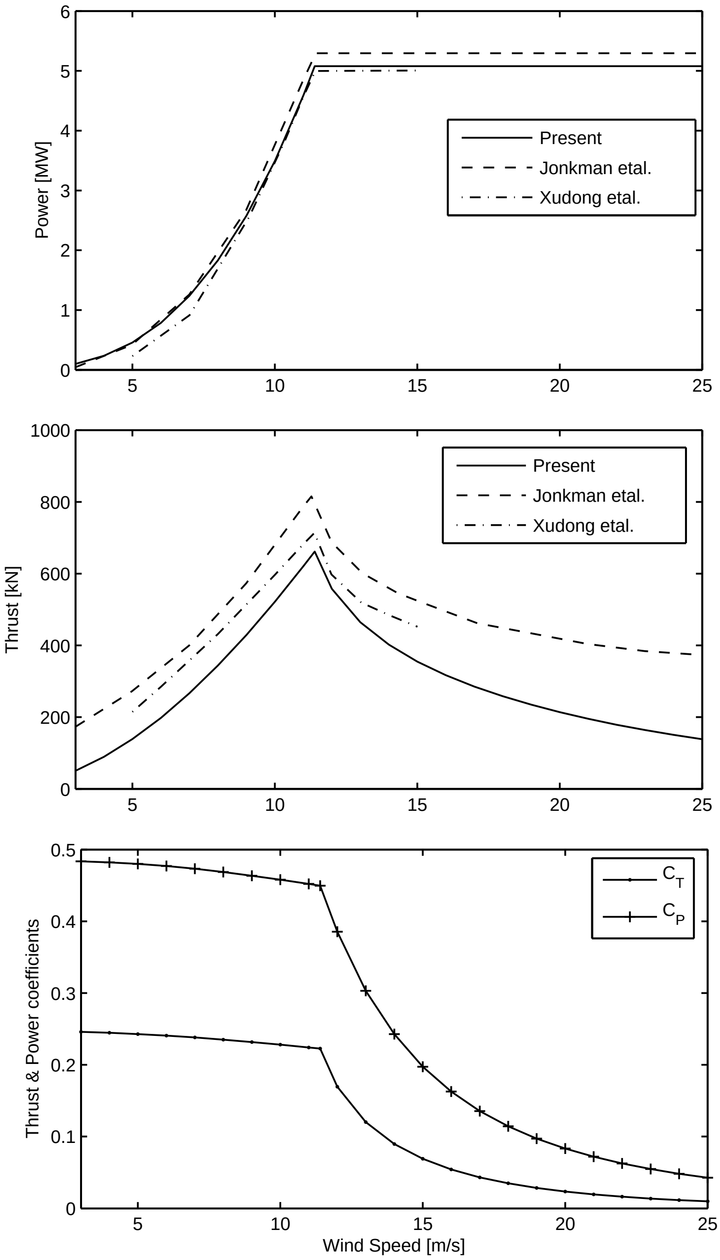

Figure 9: DRD-BEM computations for the main parameters of the NREL-RWT rotor in function of wind speed. From top to bottom: power output, thrust on the rotor's hub, and power and thrust coefficients.

	Out-of-plane deflection $[m]$	In-plane deflection $[m]$
Present	3.85	-0.56
Jonkman et al. [32]	5.47	-0.61
Xudong et al. [7]	3.53	-0.21
Jeong et al. [8]	3.76	-0.27
Kallesøe and Hansen [6]	3.24	-0.27
Yu and Kwon [9]	4.72	-0.63

Table 1: In-plane and out-of-plane deflection comparison at nominal working conditions.

blade behaves more like a slender beam. On the other hand, our results seem to indicate that in-plane deformation respond to a more complex combination of deformation modes, some of them of coupled nature, that can not be captured by classical formulations.

3.2. Blade pitch control for power limitation at wind speeds above the rated

As it was mentioned before, blade pitch control for the NREL-RWT only takes place for wind speeds above W_N. To evaluate our model in the presence of pitch control actions, we reproduced the tests reported in Jonkman et al. [32], which include computations of the *sensitivity* of aerodynamic power to blade pitch. Blade-pitch sensitivity is an aerodynamic property of the rotor which depends on wind speed, rotor speed, and blade-pith angle. It is defined as $\partial P/\partial \theta_{p_{ctr}}$, where P is the output power and $\theta_{p_{ctr}}$ is the pitch control angle.

Table 2 summarizes the results for the test, columns two and three show the optimum pitch angle and $\partial P/\partial \theta_{p_{ctr}}$ respectively.

Wind speed [m/s]	Pitch [°]	$\partial P/\partial \theta_{p_{ctr}}$ [MW/rad]
11.4 (rated)	0.00	−12.30
12.0	2.62	−20.16
13.0	5.32	−29.18
14.0	7.48	−33.86
15.0	9.27	−44.80
16.0	10.84	−50.52
17.0	12.30	−56.85
18.0	13.66	−64.09
19.0	14.95	−68.87
20.0	16.20	−72.15
21.0	17.41	−77.94
22.0	18.57	−83.81
23.0	19.68	−89.90
24.0	20.75	−95.65
25.0	21.80	−100.18

Table 2: Sensitivity of aerodynamic power to blade pitch. Generated power and rotor speed are kept constant at 5.1916 MW and 12.1 rpm respectively.

3.3. Time-dependent solutions around the nominal operational state

In what follows we show the results of time-dependent solutions from the application of our model to the analysis of the NREL-RWT operating at nominal wind speed. In order to isolate the effects of rotor deformation, tilt-angle, and gravitational forces on the aeroelastic behaviour of the rotor, in this first set of solutions we applied a constant wind speed over the entire rotor area (even though our model is capable of accepting any generic wind-profile input). When tilt is considered nil, the power predicted in the temporal solution is coincident with the value obtained for the steady state solution, which serves as a validation of the consistency of our model in its two different modes of operation. During this process, we run our model for 70 revolutions of the rotor with boundary conditions equivalent to the steady-state case. After brief warm-up period the time-dependent solution gave the exact same value as the steady-state one, with an extremely low relative *noise* of the order of 10^{-9} to 10^{-8}, which indicates the high order of precision of the method.

We analysed three cases where the factors of tilt angle, gravitational action, or a combination of both, affect the symmetry of the loads on the rotor in different ways, inducing particular modes of deformation. Figure 10 shows the time-dependent solutions for the power output for the three cases mentioned above, plus the flat solution for the case where neither tilt nor gravity are considered. For the sake of clarity, we only show a period of 4 rotor revolutions out of the total of 70 that we ran, but the pattern is repeated exactly over the total. Figure 11 shows similar results for the thrust exerted on the hub.

The effects of tilt in the rotor axis and the action of gravity are revealed by the oscillating shapes of the time-dependent solutions. The way in which tilt and gravity affect the power and the thrust curves is different, because of the main direction in which the two loads are applied. That is, the tilt angle affects the aerodynamic load which has a major component in the chord-normal direction of the blade section, while the action of gravity has a major component in the chord-wise. These different load patterns affect the shape of the oscillating curves. To provide some insight into the ways in which these shape alterations operate, we studied the time evolution of several representative parameters on individual sections along the span of the blades. A complete set of plots covering the entire blade span would be impossible to show here due to space limitations, but in figure 12 we show some examples for a particular section located at 90 % of the span from the blade root, which is quite representative of the general behaviour that we have observed. There, we show time evolution of the axial (i.e. the out-of-rotor-plane) displacement of the blade section on the hub's coordinate system $u_{str_{h_x}}$, the chord-normal component of the aerodynamic force on the blade section dF_{l_x}, and chord-wise component dF_{l_y}. It could be noticed that the oscillating pattern of forces on individual sections is much *clearer* than the ones observed at the rotor, with a kind of sinusoidal-like aspect. There is also a phase-shift present in all the plots, specially noticeable on the forces. We will return to this topic in our concluding section.

Another aspect of the fluctuations produced by tilt or gravity on power and thrust is that they are not symmetric with respect to the steady-state values computed before, and consequently, the mean values of both power and thrust are different when either of these factors are present. Table 3 shows a compilation of the mean values of power and thrust for the four cases depicted in figures 10 and 11, together with the amplitude of the associated

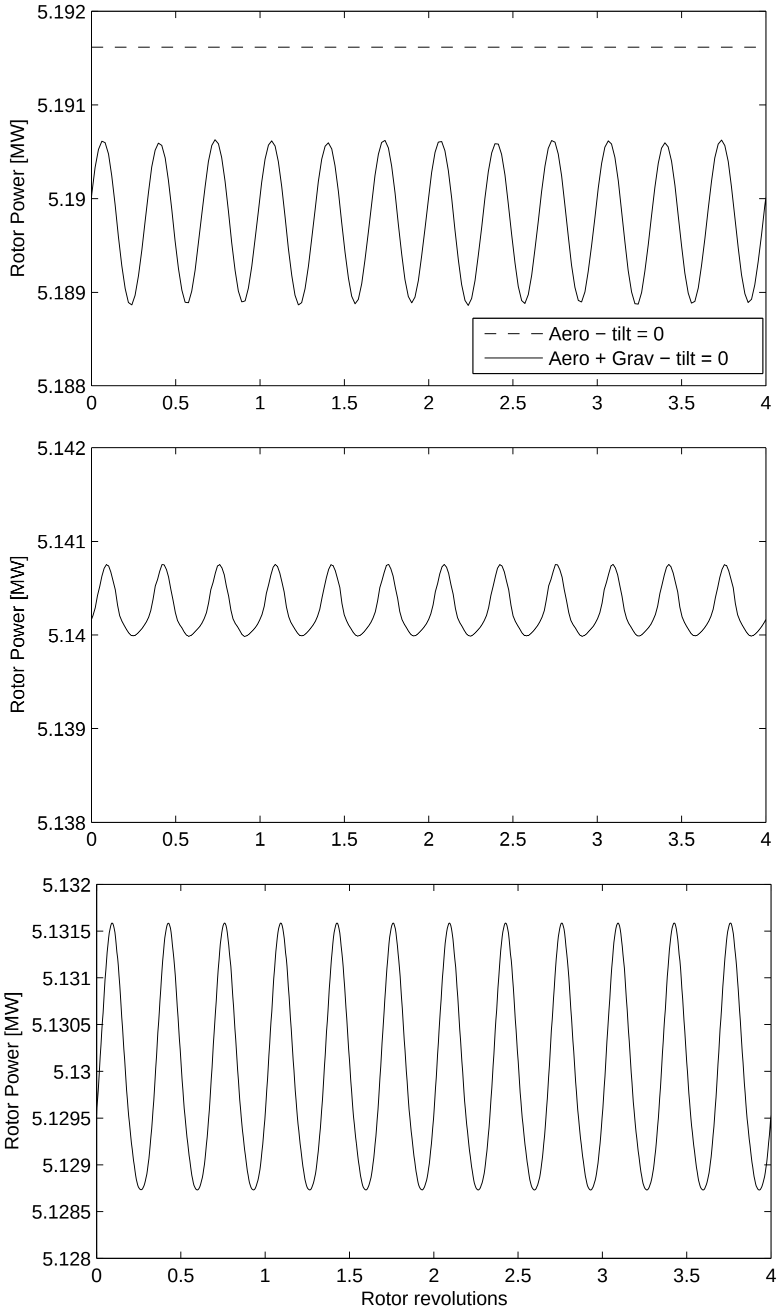

Figure 10: Time-dependent solutions for the power output of the NREL-RWT rotor under different conditions. Top panel: no-tilt aerodinamic loads, with and without gravitational loads. Mid panel: only aerodynamic loads with a 5° tilt. Bottom panel: aerodynamic and gravitational loads with a 5° tilt. The three plots have a range of 4 kW.

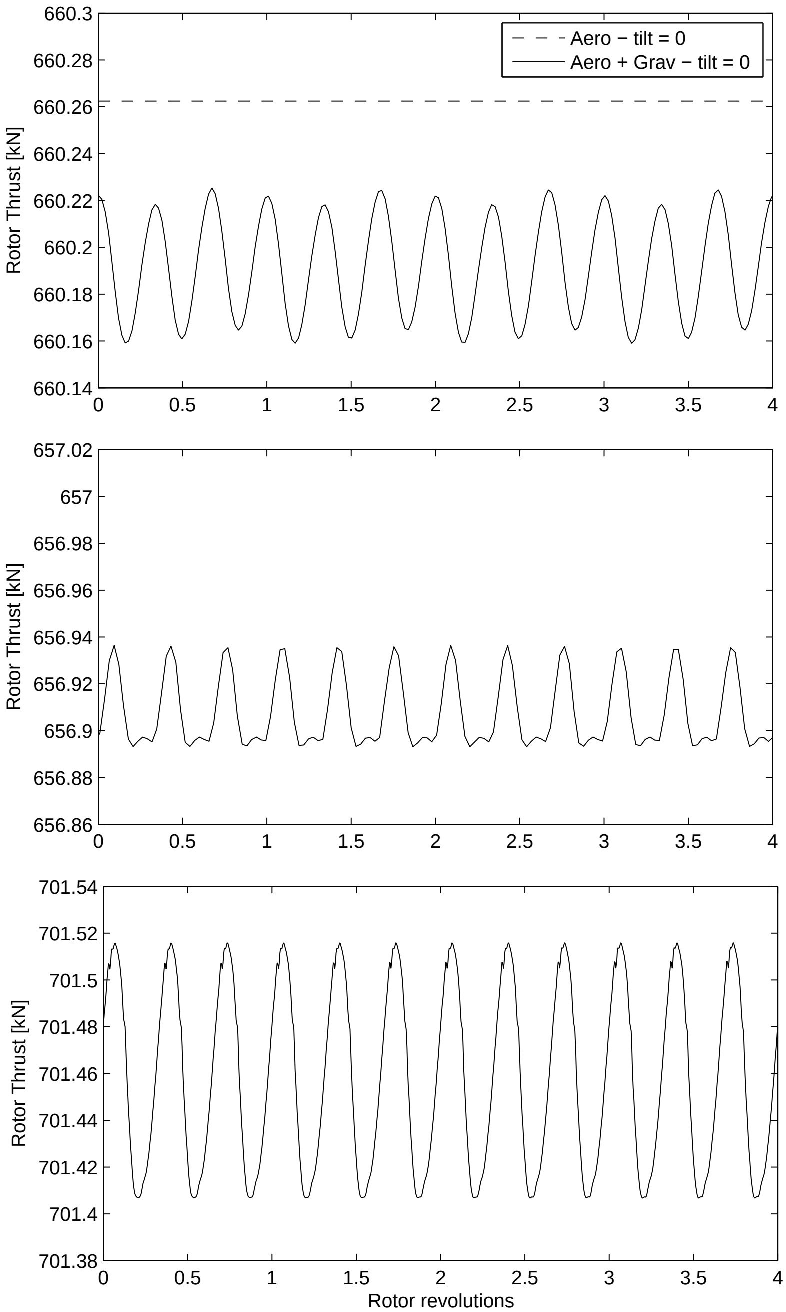

Figure 11: Time-dependent solutions for the thrust exerted on the hub of the NREL-RWT rotor under different conditions. Top panel: no-tilt aerodinamic loads, with and without gravitational loads. Mid panel: only aerodynamic loads with a 5° tilt. Bottom panel: aerodynamic and gravitational loads with a 5° tilt. The three plots have a range of 160 N.

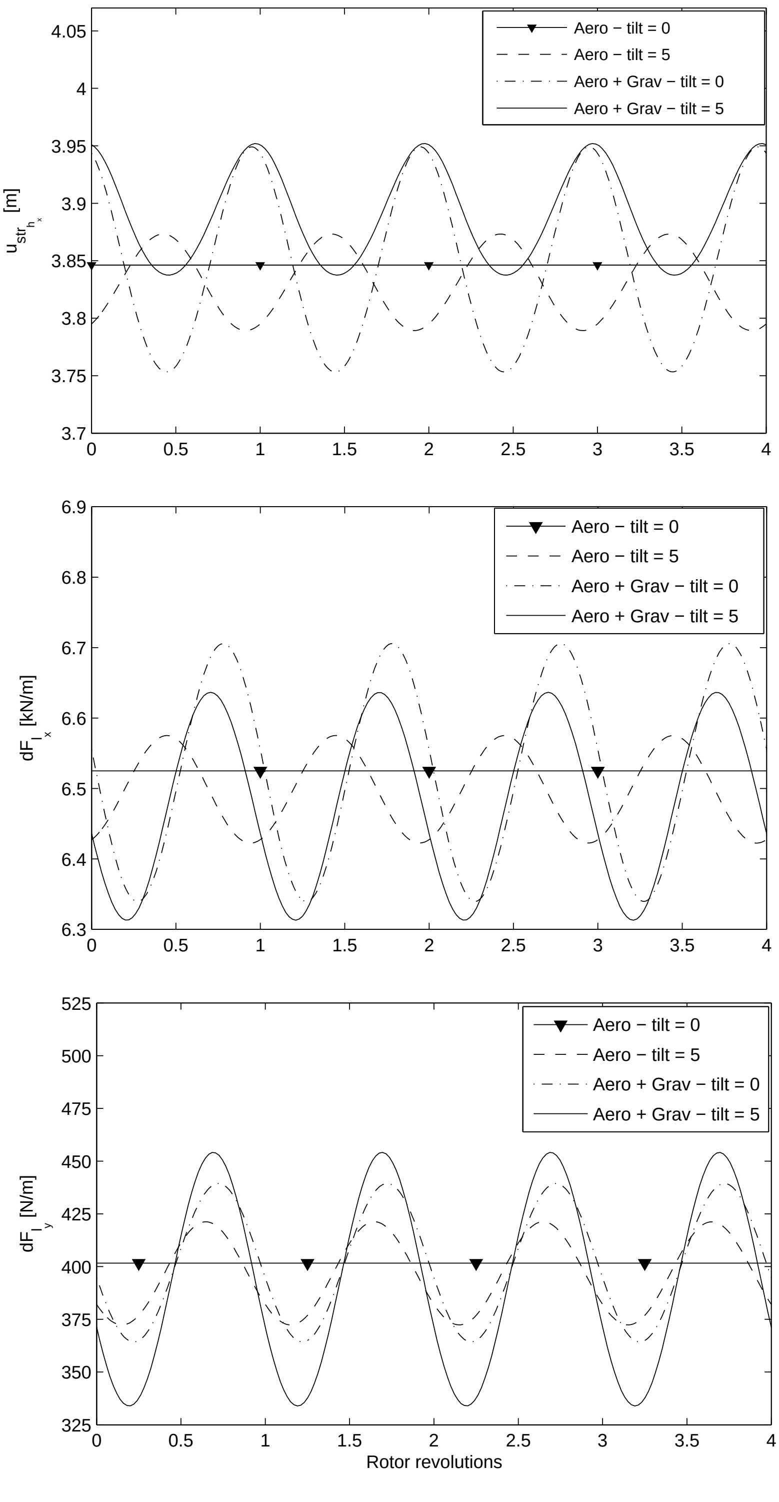

Figure 12: Time evolution for some illustrative parameters on the section of blade Nr1 located at 90 % of the span. From top to bottom: Out-of-rotor-plane displacement $u_{str_{h_x}}$, chord-normal component of the aerodynamic force dF_{l_x}, and chord-wise component dF_{l_y}.

fluctuations.

Case	Mean Power $\bar{P}$ [MW]	Power Amplitude ΔP [MW]	Mean Thrust $\bar{M}$ [kN]	Thrust Amplitude ΔM [kN]
Steady State	5.1916	-	660.26	-
Time dependent - Aero No tilt	5.1916	3.4×10^{-9}	660.26	3.9×10^{-7}
Time dependent - Aero With tilt	5.1403	9.9×10^{-4}	656.91	0.0587
Time dependent - Aero + Grav No tilt	5.1897	0.0018	660.19	0.0674
Time dependent - Aero + Grav With tilt	5.1301	0.0031	701.46	0.1324

Table 3: Power and thrust for different cases. Mean values and amplitude of oscillations.

4. Conclusions

The experiments presented here are mostly intended as validation cases using a well-known turbine design that provides an excellent benchmark for comparison. It is important to keep in mind that they reflect the fact the we are simulating a relatively stiff blade of classical construction, typical of today's commercial types. This results in relatively moderate variations on the predicted behaviour with respect to other models that do not consider the full effects of rotor deformation. However, for those cases of innovative blades mentioned in the introductory section, where stiffness is likely to be lower (and/or deformation modes to be more complex), these differences are going to be much higher, and the full capacities of our model more evident.

Nevertheless, even for this classic blade, there are several manifestations of the effects of deformation that could be observed in our data. For instance, comparing the results in table 2 with the ones reported by Jonkman et al. [32], we see that our optimum computed angles are 1° to 1.5° smaller. This is again consistent with the fact that our model takes into consideration the complex modes of deformation for the blade structure as well as its non linear behavior. On the aerodynamic side, the DRD-BEM feeds back the structural model with the corresponding re-projection of the aerodynamic loads as the structure deforms. What we see here is the result of the effect of the combined deformation modes changing the alignment of the blade sections, which causes the aerodynamic forces that produce the driving torque to decrease with increasing deformation as the wind speed increases. Thus, the pitch control angles required to maintain a constant output power turn out to be smaller than the ones predicted with models that do not consider this effects. Similarly, the values of blade-pitch sensitivity computed by our model, though in the same order of magnitude, are smaller than those predicted by Jonkman et al. [32].

Results for the time-dependent experiments in figures 10 and 11 show maximum fluctuations in a range of 160 N for the thrust and 4 kW for the power. These fluctuations are small compared with the mean values of both quantities (this is again related with the fact that we are simulating a relatively stiff blade). But, it is interesting to note that the method is still capable of capturing these small aero-elasto-inertial interactions that reflect on the contribution of the 3 blades to the total power and thrust on the rotor's hub. This is also reflected on the aerodynamic forces on individual blade sections on the external part of the blade, whose chord-normal component (mid panel figure 12) is mostly associated with the span-wise distributed force contribution to the thrust on the rotor, while its chord-wise component (bottom panel figure 12) is mostly associated with the driving torque and power output. It can be seen that the asymmetric conditions imposed by the gravitational loads and/or tilting of the nacelle produces a clearly different response with respect to the symmetric situation where these effects are disregarded. The fact that aero-elasto-inertial phenomena are actually being detected is manifested in the phase-shift of the responses with respect to the pulsating forcing applied in the cases where gravitation and/or tilt are considered.

As expected for a 3-bladed turbine, the oscillations in power and thrust depicted in figures 10 and 11 have a fundamental frequency exactly corresponding to 3 times the rotational frequency of the rotor. However, when the integrated action of the forces on all the individual sections of the 3 blades is put together, small fluctuations appear, indicating the presence of other frequencies on the spectrum. These, again, are very subtle for the case of the relatively stiff blades of the NREL-RWT. More interesting is the fact that there are clear alterations on the shape of the signals which depart from the sinusoidal-like shape shown for the distributed forces in figure 12, whose origin could be attributed to the combined effect of different phase-shifts on the many sections along the span of the 3 blades. This may be an indication that, even in the case where the load fluctuation on individual sections may be simple in terms of phase and frequency content, the overall action of the deformation modes along the span of the three blades on the rotor would create more complex patterns of fluctuation for general parameters on the hub like power, torque, and thrust. This may prove important for the design of mechanical components on the drive train like bearings, and gear boxes, and for the determination of their expected operational life.

The capability of our code of capturing even these small fluctuating components on the NREL-RWT opens the door to future detailed analysis of this kind of problems in cases where those effects would be more substantial. These may include cases of larger blades (where the fluctuating forces associated with gravity are likely to become critical in terms of fatigue effects [15]); or cases of innovative blades of novel design, like relatively lighter blades of softer construction, or adaptive blades with complex aeroelastic combined modes of deformation.

5. Acknowledgments

The authors are very grateful for the financial support made available by the National Science Foundation through grants CEBET-0933058 and CEBET-0952218, by University of Buenos Aires through grant 20020100100536 UBACyT 2011/14, and and by CONICET through grant PIP 11220120100480CO.

[1] Ponta, F.L., Otero, A.D., Rajan, A., Lago, L.I.. The adaptive-blade concept in wind-power applications. Energy for Sustainable Development 2014;22(0):3 – 12. doi:\bibinfo{doi}{http://dx.doi.org/10.1016/j.esd.2014.04.004}. Wind Power Special Issue.

[2] Hansen, M.O.L., Sørensen, J.N., Vousitas, S., Sørensen, N., Madsen, H.A.. State of the art in wind turbine aerodynamics and aeroelasticity. Prog in Aerospace Sciences 2006;42:285–330.

[3] Jonkman, J.M., Buhl Jr, M.L.. Fast user's guide. Tech. Rep. NREL/EL-500-38230; National Renewable Energy Laboratory (NREL); Golden, Colorado, USA; 2005. URL `http://wind.nrel.gov/designcodes/simulators/fast`.

[4] Moriarty, P., Hansen, A., (US), N.R.E.L., Engineering, W.. Aerodyn theory manual. National Renewable Energy Laboratory; 2005.

[5] Laino, D., Hansen, A.. User's guide to the wind turbine aerodynamics computer software aerodyn. Tech. Rep.; National Renewable Energy Laboratory under subcontract No. TCX-9-29209-01; 2002.

[6] Kallesøe, B.S., Hansen, M.H.. Effects of large bending deflections on blade flutter limits. Tech. Rep.; Danmarks Tekniske Universitet, Risø Nationallaboratoriet for Bæredygtig Energi; 2008.

[7] Xudong, W., Shen, W.Z., Zhu, W.J., Srensen, J.N., Jin, C.. Shape optimization of wind turbine blades. Wind Energy 2009;12(8):781–803.

[8] Jeong, M.S., Yoo, S.J., Lee, I.. Aeroelastic analysis for large wind turbine rotor blades. In: 52nd AIAA/ASME/ASCE/AHS/ASC Structures, Structural Dynamics and Materials Conference 19th AIAA/ASME/AHS Adaptive Structures Conference 13t. 2011, p. 1950.

[9] Yu, D.O., Kwon, O.J.. Predicting wind turbine blade loads and aeroelastic response using a coupled cfdcsd method. Renewable Energy 2014;70:184 – 196. Special issue on aerodynamics of offshore wind energy systems and wakes.

[10] Bazilevs, Y., Hsu, M.C., Akkerman, I., Wright, S., Takizawa, K., Henicke, B., et al. 3d simulation of wind turbine rotors at full scale. part i: Geometry modeling and aerodynamics. International Journal for Numerical Methods in Fluids 2011;65(1-3):207–235. doi:\bibinfo{doi}{10.1002/fld.2400}. URL `http://dx.doi.org/10.1002/fld.2400`.

[11] Bazilevs, Y., Hsu, M.C., Kiendl, J., Wchner, R., Bletzinger, K.U.. 3d simulation of wind turbine rotors at full scale. part ii: Fluid-structure interaction modeling with composite blades. International Journal for Numerical Methods in Fluids 2011;65(1-3):236–253. doi:\bibinfo{doi}{10.1002/fld.2454}. URL `http://dx.doi.org/10.1002/fld.2454`.

[12] Sorensen, J.N., Shen, W.Z.. Numerical modeling of wind turbine wakes. Journal of fluids engineering 2002;124(2):393–399.

[13] Otero, A.D., Ponta, F.L.. Structural analysis of wind-turbine blades by a generalized Timoshenko beam model. Journal of Solar Energy Engineering 2010;132(1):011015. doi:\bibinfo{doi}{10.1115/1.4000596}.

[14] Ponta, F.L., Jacovkis, P.M.. A vortex model for Darrieus turbine using finite element techniques. Renewable Energy 2001;24:1–18.

[15] Manwell, J.F., McGowan, J.G., Rogers, A.L.. Wind energy explained: Theory, design and application. Chichester, UK: Wiley; 2002.

[16] Burton, T., Sharpe, D., Jenkins, N., Bossanyi, E.. Wind Energy Handbook. Chichester, UK: Wiley; 2001.

[17] Glauert, H.. A general theory of the autogyro. Aeronautical Research Committee – HM Stationery Office; 1926.

[18] Glauert, H.. Airplane propellers. In: Aerodynamic theory. Springer; 1935, p. 169–360.

[19] Crawford, C.. Re-examining the precepts of the blade element momentum theory for coning rotors. Wind Energy 2006;9(5):457–478.

[20] Lanzafame, R., Messina, M.. Fluid dynamics wind turbine design: Critical analysis, optimization and application of {BEM} theory. Renewable Energy 2007;32(14):2291 – 2305. doi:\bibinfo{doi}{http://dx.doi.org/10.1016/j.renene.2006.12.010}.

[21] Lanzafame, R., Messina, M.. {BEM} theory: How to take into account the radial flow inside of a 1-d numerical code. Renewable Energy 2012;39(1):440 – 446. doi:\bibinfo{doi}{http://dx.doi.org/10.1016/j.renene.2011.08.008}.

[22] Madsen, H.A., Mikkelsen, R., Øye, S., Bak, C., Johansen, J.. A detailed investigation of the blade element momentum (bem) model based on analytical and numerical results and proposal for modifications of the bem model. In: Journal of Physics: Conference Series; vol. 75. IOP Publishing;

2007, p. 012016.

[23] Dai, J., Hu, Y., Liu, D., Long, X.. Aerodynamic loads calculation and analysis for large scale wind turbine based on combining {BEM} modified theory with dynamic stall model. Renewable Energy 2011;36(3):1095 – 1104. doi:\bibinfo{doi}{http://dx.doi.org/10.1016/j.renene.2010.08.024}.

[24] Leishman, J., Beddoes, T.. A generalised model for airfoil unsteady aerodynamic behaviour and dynamic stall using the indicial method. In: 42nd. Annual Forum of the American Helicopter Society, Washington D. C. 1986,.

[25] Vaz, J.R.P., Pinho, J.T., Mesquita, A.L.A.. An extension of {BEM} method applied to horizontal-axis wind turbine design. Renewable Energy 2011;36(6):1734 – 1740. doi:\bibinfo{doi}{http://dx.doi.org/10.1016/j.renene.2010.11.018}.

[26] Hansen, M.. Aerodynamics of wind turbines. Earthscan/James & James; 2008.

[27] IEC, . Wind turbine generator systems – part 13: Measurement of mechanical loads. Report IEC/TS 61400–13; International Electrotechnical Commission (IEC); 2001.

[28] Griffin, D.A.. Blade system design studies volume I: Composite technologies for large wind turbine blades. Report SAND2002-1879; Sandia National Laboratories; 2002.

[29] Yu, W., Hodges, D.H.. Generalized Timoshenko theory of the variational asymptotic beam sectional analysis. J American Helicopter Society 2005;50:46–55.

[30] Yu, W., Hodges, D.H., Volovoi, V., Cesnik, C.E.S.. On Timoshenko-like modeling of initially curved and twisted composite beams. Int J Sol and Struct 2002;39:5101–5121.

[31] Hodges, D.H.. Nonlinear Composite Beam Theory. Reston, Virginia: AIAA; 2006.

[32] Jonkman, J., Butterfield, S., Musial, W., Scott, G.. Definition of a 5-MW reference wind turbine for offshore system development. Tech. Rep. NREL/TP-500-38060; National Renewable Energy Laboratory; 2009.

[33] Jamieson, P.. Innovation in wind turbine design. Wiley; 2011.

[34] Crawford, C., Platts, J.. Updating and optimization of a coning rotor concept. Journal of Solar Energy Engineering 2008;130:031002.

[35] Burden, R.L., Faires, J.D.. Numerical analysis. Brooks Cole; 1998.

[36] Mathews, J.H., Fink, K.D.. Numerical methods using Matlab. Prentice Hall; 1999.

[37] Du, Z., Selig, M.S.. A 3-D stall-delay model for horizontal axis wind turbine performance prediction. In: AIAA, Aerospace Sciences Meeting and Exhibit, 36 th, and 1998 ASME Wind Energy Symposium; vol. 21. American Institute of Aeronautics and Astronautics, Inc./ASME International; 1998, p. 9–19.

[38] Eggers, A.. Modeling of yawing and furling behavior of small wind turbines. In: 2000 ASME Wind Energy Symposium, 19 th, AIAA, Aerospace Sciences Meeting and Exhibit, 38 th, Reno, NV. 2000, p. 1–11.

[39] Leishman, J., Aerodynamicist, S., Beddoes, T., Specialist, A.. A Semi-Empirical Model for Dynamic Stall. Journal of the American Helicopter Society 1989;34:3.

[40] Leishman, J., Beddoes, T.. A generalized model for unsteady aerodynamic behaviour and dynamic stall using the indicial method. J Am Helicopter Soc 1990;36:14–24.

[41] Viterna, L.A., Janetzke, D.C.. Theoretical and experimental power from large horizontal-axis wind turbines. Tech. Rep.; National Aeronautics and Space Administration, Cleveland, OH (USA). Lewis Research Center; 1982.

[42] Buhl, M.. A new empirical relationship between thrust coefficient and induction factor for the turbulent windmill state. Tech. Rep.; National Renewable Energy Laboratory; 2005.

[43] Lock, C.N.H., Bateman, H., Townend, H.. An extension of the vortex theory of airscrews with applications to airscrews of small pitch, including experimental results. Aeronautical Research Committee, R&M, HM Stationery Office 1925;1014:1–49.

[44] Wilson, R.. Aerodynamic behavior of wind turbines. In: Spera, D., editor. Wind Turbine Technology, Fundamental Concepts of Wind Turbine Engineering. 1994,.

[45] Bak, C., Aagaard Madsen, H., Johansen, J.. Influence from blade-tower interaction on fatigue loads and dynamic (poster). In: Wind energy for the new millennium. Proceedings. 2001 European wind energy conference and exhibition (EWEC'01). 2001, p. 2–6.

[46] Powles, S.R.J.. The effects of tower shadow on the dynamics of a horizontal-axis wind turbine. Wind Engineering 1983;7:26–42.
[47] Otero, A.D., Ponta, F.L., Lago, L.I.. Structural analysis of complex wind turbine blades: Flexo-torsional vibrational modes. In: Carriveau, R., editor. Advances in Wind Power. InTech. ISBN 978-953-510-863-4; 2012,.
[48] Lago, L.I., Ponta, F.L., Otero, A.D.. Analysis of alternative adaptive geometrical configurations for the NREL-5 MW wind turbine blade. Renewable Energy 2013;59:13 – 22.
[49] Øye, S.. Flex4 simulation of wind turbine dynamics. In: Proceedings of the 28th IEA Meeting of Experts Concerning State of the Art of Aeroelastic Codes for Wind Turbine Calculations (Available through International Energy Agency). 1996,.